analytical chemistry

pubs.acs.org/ac Article

Spatially Offset Raman Spectroscopy—How Deep?

Sara Mosca, Priyanka Dey, Marzieh Salimi, Benjamin Gardner, Francesca Palombo, Nick Stone,* and Pavel Matousek*

Cite This: https://doi.org/10.1021/acs.analchem.1c00490 Read Online

ACCESS | Metrics & More | Article Recommendations | Supporting Information

ABSTRACT: Spatially offset Raman spectroscopy (SORS) is a technique for interrogating the subsurface composition of turbid samples noninvasively. This study generically addresses a fundamental question relevant to a wide range of SORS studies, which is how deep SORS probes for any specific spatial offset when analyzing a turbid sample or, in turn, what magnitude of spatial offset one should select to probe a specific depth. This issue is addressed by using Monte Carlo simulations, under the assumption of negligible absorption, which establishes that the key parameter governing the extent of the probed zone for a point-like illumination and point-like collection SORS geometry is the reduced scattering coefficient of the medium. This can either be deduced from literature data or directly estimated from a SORS measurement by evaluating the Raman intensity profile from multiple spatial offsets. Once this is known, the extent of the probed zone can be determined for any specific SORS spatial offset using the Monte Carlo simulation results presented here. The proposed method was tested using experimental data on stratified samples by analyzing the signal detected from a thin layer that was moved through a stack of layers using both non-absorbing and absorbing samples. The proposed simple methodology provides important additional information on SORS measurements with direct relevance to a wide range of SORS applications including biomedical, pharmaceutical, security, forensics, and cultural heritage.

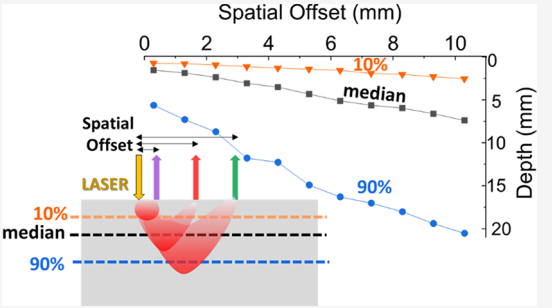

INTRODUCTION

Spatially offset Raman spectroscopy (SORS)[1−3] has proven to be a useful analytical tool for determining the subsurface chemical composition of turbid samples, with applications ranging from disease diagnosis[4] to security screening and quality control in the pharmaceutical industry or analysis of objects of art through layer(s) of paint. SORS relies on the separation between the illumination and collection zones on a sample surface.[2] The larger the separation (spatial offset, Δs), the greater the depth from which the Raman signal can be retrieved.[5] This is due to the fact that sideways photon migration is statistically biased toward deeper zones, favoring photon pathways that stay away from the lossy air-to-sample interface. This is because if any photon migrates close to this interface, it has a high likelihood of crossing the boundary and escaping irretrievably from the sample.[6]

Despite the wide range of applications and associated research, one important question has yet to be generically addressed, i.e., determining the extent of the probed zone for any specific SORS offset for a given sample. Answering this question also enables one to select an optimum spatial offset for probing a specific depth. Although a number of studies have been carried out to elucidate the extent of the SORS-probed region, these were performed for specific sample situations, not providing generic guidance on other cases.[7−9] A further highly comprehensive analysis including absorption properties was carried out using Monte Carlo (MC) simulations focusing on skin probing properties.[10] Although the study provides rich information on the sampling volume for different combinations of reduced scattering and absorption coefficients, it investigates only a single SORS spatial offset (0.4 mm) tailored to shallow depth skin investigations. Other similar studies were carried out for conventional Raman spectroscopy.[11] Here, we aim to provide a simple, widely implementable methodology for estimating the probed depth and its extent applicable across all spatial scales without the need to perform MC calculations. The method is valid under the assumption of negligible absorption (i.e., diffusion approximation[12,13]) and a homogeneous sample, which is a requirement satisfied in a range of SORS investigations in the near-infrared region of spectra.

The approach consists of two distinct steps. The first approach is determining the reduced scattering coefficient of the probed sample. This can be accomplished using the SORS Raman intensity decay profile with increasing spatial offset, as described in our recent publication,[14] by performing other measurements (e.g., continuous[15] and/or time-resolved[16,17]

Received: February 2, 2021
Accepted: April 12, 2021

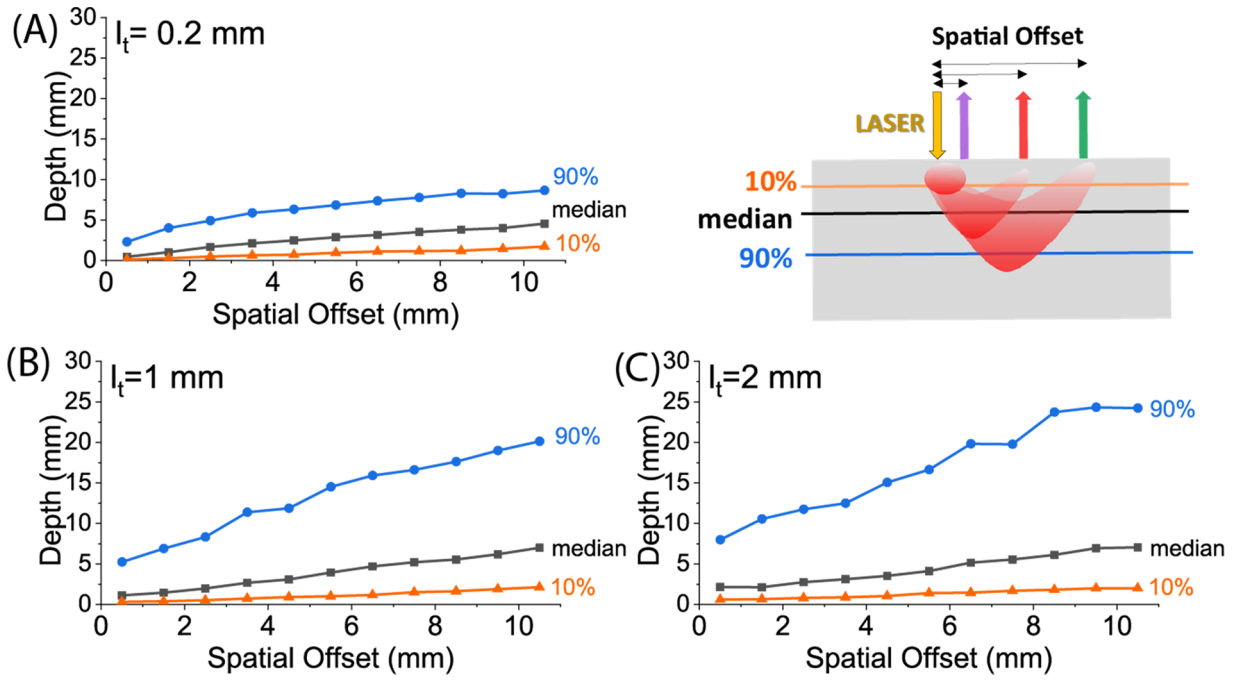

Figure 1. Plots of 10%, 50% (median), and 90% quantile depths versus spatial offset derived from the Monte Carlo simulations for three representative transport lengths: (A) l_t = 0.2 mm (μ_s' = 5 mm^{-1}), (B) l_t = 1 mm (μ_s' = 1 mm^{-1}), and (C) l_t = 2 mm (μ_s' = 0.5 mm^{-1}).

diffuse IR) or obtained from literature data.[18,19] The second approach is assigning appropriate probed depth parameters to each spatial offset from the results of numerical simulations provided here.

The calculated SORS-probed depth is given as a probed median depth for each spatial offset, delineating a boundary between half of the Raman photons originating from above the boundary and the other half from below this boundary. The calculations also provide 10 and 90% quantile depths. With the 10% quantile, 10% of detected Raman photons originate from this depth and shallower. Correspondingly, with the 90% quantile, 90% photons originate from this depth and shallower. The knowledge of these parameters is often crucially important in a wide range of SORS measurements linking the observed Raman signals with any specific zone within the probed matrix.[20−22] We have tested the prediction using experimental data derived from a segmented sample where an interlayer of different chemical makeup was moved throughout a stack of layers. The study was performed using both non-absorbing and absorbing samples.

MONTE CARLO SIMULATIONS

MC simulations[23] were used to evaluate the extent of the SORS-probed zone. The code has been described in detail earlier.[1,14] Briefly, both the laser and Raman photons were propagated through a turbid medium in the three-dimensional space. In each step, a photon was propagated through a straight line over a transport length distance, l_t , and thereafter, its direction was randomized.[24,25] The transport length is related to the medium's reduced scattering coefficient (μ_s') by $l_t = 1/\mu_s'$. Each sample was assumed to be homogeneous and semi-infinite, with a single sample-to-air interface at the illumination and Raman collection side. The laser photons were initially placed at a depth equal to the transport length l_t and uniformly distributed across the illumination spot of radius r. To ensure the effective yield of Raman photons, these were collected in the SORS circular collection geometry through concentric annuli. To ensure its widest applicability across multiple spatial scales, the model aimed to approximate an ideal system for which the extent of the spatial offset determined by the width of the collection annulus and dimension of the illumination area is much smaller than the transport length of the sample. For practical reasons, this often cannot be fully satisfied since a finite collection area is required to collect a sufficiently large number of Raman photons for any specific spatial offset (both in MC simulations and actual experiments), and so, the model only represents an approximation of such an ideal system. Although the MC simulations were carried out in circular collection geometry, all the derived depth parameters are identical at corresponding spatial offsets for both the point-like illumination and collection geometry as well as for a ring illumination and point-like collection geometry (inverse SORS). The numerical code was written in Mathematica 9.0.1.0 (Wolfram Research). A total of 2,000,000 photons were propagated simultaneously, each over 10,000 steps with a step size of l_t. The transport length (step size) was varied from 0.2 to 2.0 mm. To maximize the computational efficiency, the conversion coefficient accounting for the conversion of laser photons to Raman photons was set at 0.00023 mm^{-1} (optical density OD = 0.00010 mm^{-1}), a value that is unrealistically high. However, since the spontaneous Raman spectroscopy is a linear process, the relative Raman intensities generated, and of interest here, are unaffected. Although some inaccuracies can be present due to laser beam depletion toward the end of photon propagation, the variation of this parameter however did not reveal any significant effects of this depletion on the calculated values. Unless stated otherwise, the basic conditions were as follows: the probe beam radius was r = 1 μm (to represent the ideal point-like illumination for the widest utility of the drawn conclusions) and the sample was assumed to be homogeneous and non-absorbing at both the laser and Raman wavelengths. The photons were collected through annuli of 1

https://doi.org/10.1021/acs.analchem.1c00490
Anal. Chem. XXXX, XXX, XXX−XXX

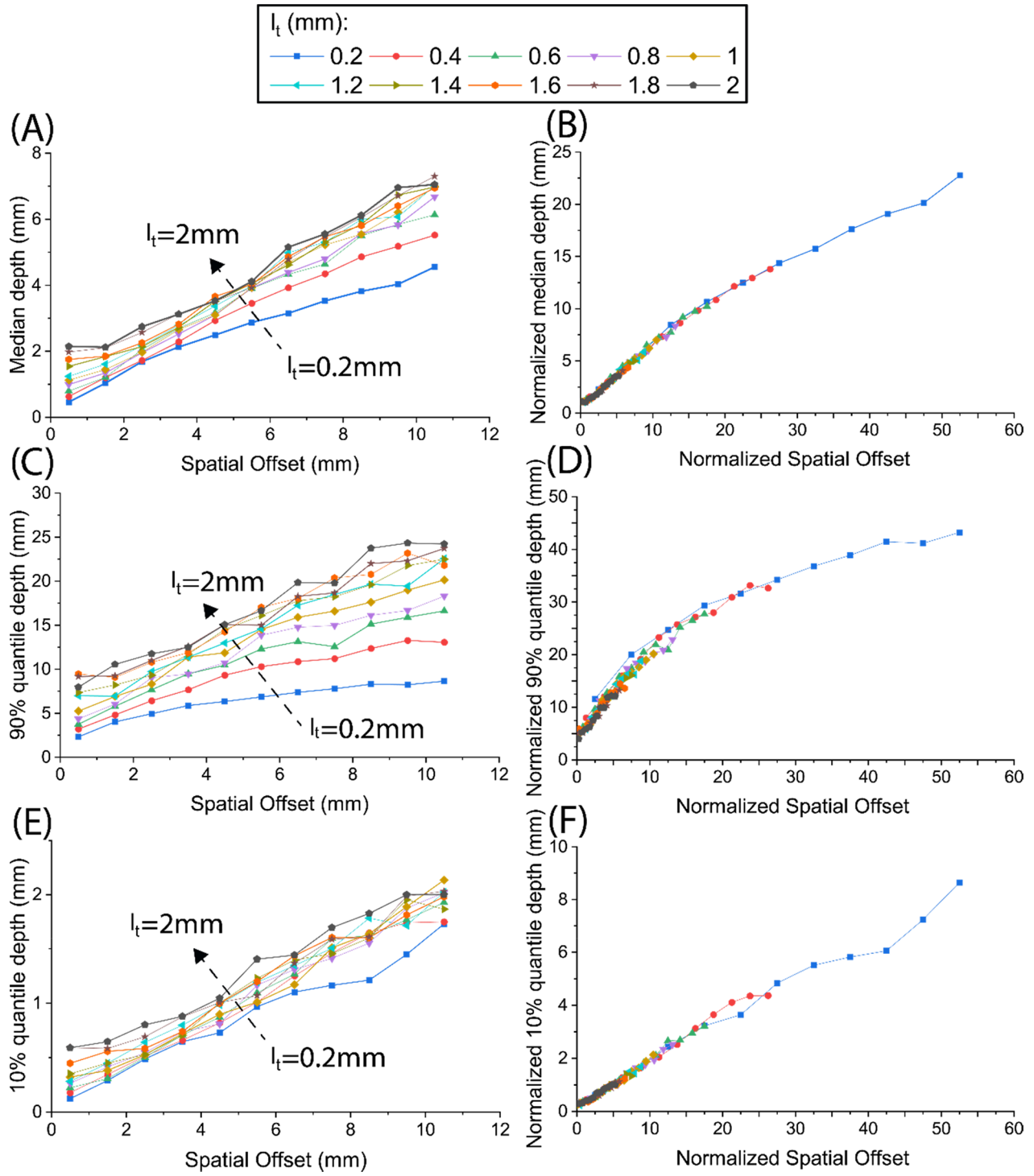

Figure 2. Left panel: (A) median, (C) 90%, and (E) 10% quantile depths versus spatial offset calculated from the Monte Carlo simulations for different sample transport lengths. Right panel: dimensionless representation where l_t dependencies are largely removed (within the accuracy of the modeling): (B) median, (D) 90%, and (F) 10% quantile depths are normalized to transport length l_t (i.e., depth/l_t) and plotted versus normalized spatial offset (SO/l_t) for different sample transport lengths. The legend above applies to all the graphs.

mm width each. The spatial offset assigned to each annulus, Δs, was defined as the radius of the center of the annulus (i.e., the arithmetic average of the annulus radius boundaries[14]).

RESULTS OF NUMERICAL SIMULATIONS

Figure 1 exemplifies the dependencies of the median depth and the 10 and 90% quantile depths, illustrating the depth from which the Raman signal originates for each SORS spatial offset. Three different examples are given for different transport lengths of the probed matrix. All depth parameters show an increase with increasing spatial offset, as expected, reflecting the fundamental property of SORS that the increase in spatial offset leads to probing deeper inside the matrix. By comparing the plots for different transport lengths, it transpires that the median depth (i.e., 50% quantile depth) and 90% quantile depth exhibit a relatively strong increase with the transport

https://doi.org/10.1021/acs.analchem.1c00490
Anal. Chem. XXXX, XXX, XXX−XXX

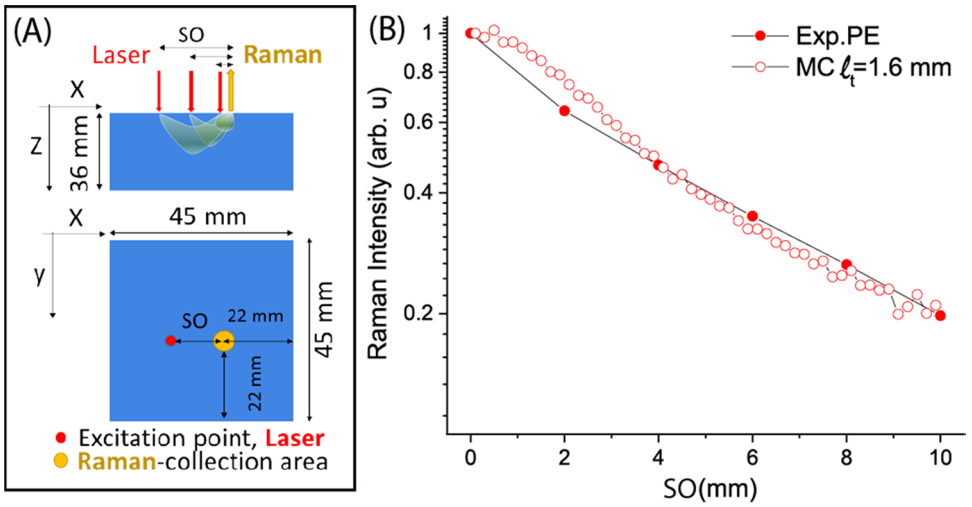

Figure 3. (A) Schematic of the model sample and SORS experimental configuration. (B) Plot of the Raman intensity decay versus SORS spatial offset (SO), measured for the PE sample (filled circles) and derived from Monte Carlo simulations for l_t = 1.6 mm (empty circles).

length. In contrast, a weaker dependence on the transport length is observed for the 10% quantile depth. For example, for transport length l_t = 1 mm, which is not too dissimilar to those of many biological tissues[26,27] (Figure 1B), a 4.5 mm spatial offset probes a median depth of 3.1 mm with 90% of Raman photons originating from 12 mm depth or shallower. Only 10% of Raman photons originate from 0.9 mm depth or shallower.

These parameters increase for the 10.5 mm spatial offset to 7.0 mm (median), 20 mm (90% quantile), and 2.1 mm (10% quantile) depths. The above median and quantile values also enable the strength of Raman signal from stratified samples to be estimated in certain situations and under the above assumptions too. For example, in the case of a two-layer medium with the top layer (overlayer) of thickness equal to the 90% quantile depth (for a particular spatial offset) located on top of an infinitely deep sublayer of similar scattering properties and Raman cross section, the sublayer would constitute 10% of Raman intensity and the overlayer would constitute 90% of Raman intensity detected overall at this specific spatial offset.

The same can be stated for the median depth. In this case, the overlayer of the median depth thickness for a specific spatial offset and an infinitely deep sublayer would yield Raman signals of equal strengths for the corresponding spatial offset. The same applies in analogy to the 10% quantile depth. As stated above, to derive the above depth parameters, one needs to first establish the reduced scattering coefficient, μ_s', or transport length, l_t , of the medium ($l_t = 1/\mu_s'$). This can be obtained from literature data, e.g., from IR diffusion measurements,[18,28−30] or derived from SORS measurements themselves as demonstrated in our recent study.[14] The SORS measurement is based on measuring the rate of decrease of the Raman signal with increasing spatial offset and applies to non-absorbing homogeneous samples. As this rate is strongly transport length-dependent, one can assign a specific transport length to the observed decay rate of Raman signal. Knowing this parameter, one can then assign the above probed depths to any specific spatial offset using the numerical data presented here (Figure 2).

The left column in Figure 2 (i.e., A, C, and E) shows the median, 90%, and 10% quantile depths versus SORS spatial offset plotted individually for a range of transport lengths found in common turbid samples (e.g., biological tissues, plastic materials, and powders). The right column in Figure 2 (i.e., B, D, and F) gives the same quantities, as well as the spatial offset expressed as a multiple of the transport length of the matrix, i.e., in a dimensionless frame (normalized spatial offset = $\Delta s/l_t = \Delta s \cdot \mu_s'$). In this representation, all the dependencies on transport length vanish within the above-mentioned approximation and calculation accuracies. This evidences that the transport length defines the scale of the problem, and the variation of the dependence of the depth properties is solely due to the transport length, in a similar way that absolute intensities do with the SORS spatial offset as shown earlier.[14] In other words, it is the transport lengths (or reduced scattering coefficient, $l_t = 1/\mu_s'$) that defines the scale of the problem, and when all the spatial variables are expressed as multiples of the transport length, all the dependencies on transport length vanish (note that the small residual dependence on transport length for the 90% quantile profile is assigned to the fact that the assumed collection system does not have an infinitely small width of the collection annulus, giving a range of spatial offsets within it that is comparable to the transport length, especially for the smallest values of transport length where the small departure from the common trend is the most pronounced).

Overall, within such a representation, all SORS systems under the above assumptions behave identically in terms of the extent of the probed depth (also expressed as a multiple of transport length).

EXPERIMENTAL SECTION

To test the prediction of the theory, we performed a range of experiments on stratified samples where a chemically distinct thin interlayer was moved through a stack of plastic layers to ascertain the SORS-probed depths. The experiments were performed using a SORS setup described previously.[22] Briefly, the excitation source was a near-infrared (NIR) diode laser with an 830 nm wavelength and 200 mW output power at the sample. The laser illumination spot on the sample surface had a diameter of ∼0.5 mm, while the Raman signal was collected in a point-like SORS configuration from a spot with an ∼1.5 mm diameter. The Raman spectra were acquired with an acquisition time of 10 s and six accumulations (i.e., total

https://doi.org/10.1021/acs.analchem.1c00490
Anal. Chem. XXXX, XXX, XXX−XXX

time 60 s) for different spatial offsets. The SORS spatial offset was defined as the distance between the centers of the illumination and collection zones on the sample surface. Synthetic model phantom samples were used as turbid media: polyethylene (PE) ($x\ y\ z$ = 45 × 45 × 36 mm^3), polystyrene (PS) ($x\ y\ z$ = 45 × 45 × 26 mm^3), and a thin sheet of polytetrafluoroethylene (PTFE) used as a target layer ($x\ y\ z$ = 45 × 45 × 1 mm^3). The intensities of the main Raman bands for each sample (PE: 1070 cm^{-1}; PS: 1003 cm^{-1}; PTFE: 734 cm^{-1}) were evaluated as the areas of Gaussian curves derived from a fit analysis of the peaks for different spatial offsets.

EXPERIMENTAL RESULTS AND DISCUSSION

As discussed above, the first step of the proposed method consists of finding the transport length (or reduced scattering coefficient) of the probed sample, e.g., by evaluating the SORS intensity decay rate with increasing spatial offset[14] or using literature data. In this study, we conducted SORS measurements by first acquiring the SORS spectra at different spatial offsets (SO = 0, 2, 4, 6, 8, and 10 mm) for the matrix alone, polyethylene (PE homogeneous slab; schematic in Figure 3A). Figure 3B shows the decay of Raman intensity with a spatial offset (SO), given as the base-10 logarithm of the intensity of the 1070 cm^{-1} Raman band as a function of the SORS spatial offset. Using a calibration model and the prediction method described in our previous work,[14] we estimated the reduced scattering coefficient of PE to be μ_s' = 0.61 mm^{-1}. This corresponds to a transport length l_t of 1.63 mm. It is noted that this value is consistent with a reported nominal value in the NIR spectral region[31] (see Figure S1, Supporting Information).

As a cross-check, we also overlapped the experimental intensity decay profile for PE with a decay profile obtained from the Monte Carlo simulations for a material with a similar l_t value (1.6 mm), achieving a satisfactory match confirming the validity of the used MC model (Figure 3B). The remaining differences present (Figure S2, Supporting Information) can be assigned largely to the fact that our SORS system is only a crude approximation of a point-like ideal SORS configuration used in the MC simulations.[14]

In the second set of experiments, we monitored a Raman spectrum of a 1 mm-thick layer of PTFE (interlayer) placed inside a PE turbid matrix made of a stack of PE sheets (each 3 mm thick) at different depths. The SORS spectra were acquired for different spatial offsets (SO = 0, 2.5, 5, and 10 mm) (see schematics in Figure 4). The resulting plots of Raman intensities of the PTFE interlayer (at 734 cm^{-1}) versus depth in the matrix are shown in Figure 5 for representative spatial offsets.

A very good correspondence between the experimental results and numerical simulations was observed for the spatial offsets of 0 and 5 mm. (A small mismatch between the MC simulations and experimental values of spatial offsets used is noted. This is due to unintentional sampling of different grid points in each case and not for any specific physical reason. The difference in spatial offsets used when comparing results is small (0.5 mm) and not believed to be significant when comparing the results.)

A small deviation between the reduced probed depth observed experimentally and that derived from Monte Carlo simulations was observed for the largest spatial offset (10 mm). The difference was attributed to either the use of an inaccurate value of absorption coefficient of the matrix (10^{-5} mm^{-1}, which was obtained from a separate time-resolved near-infrared measurement;[26,32] the Role of Absorption section and Figures S2 and S4 in the Supporting Information) or to boundary effects stemming from the fact that the medium is not semi-infinite (Figure 3A) and photons are lost on the sample side and at the bottom interface. Additionally, the non-point-like SORS configuration of the experimental setup could also play some role. In all cases, median (i.e., 50%), 10%, and 90% quantiles are indicated for each offset, evidencing acceptable correspondence between the theory and experiment.

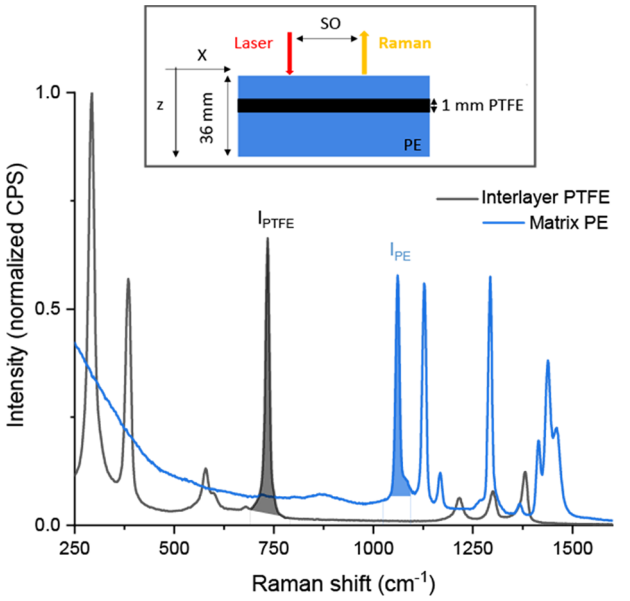

Figure 4. Upper panel: schematic of the experiment. Lower panel: micro-Raman spectra of PE (blue line) used as a turbid matrix and PTFE (black line) used as a thin interlayer placed in the turbid matrix at different depths. The shaded areas highlight the Raman bands used to evaluate the Raman intensity for each component.

Interestingly, for the 10 mm spatial offset (Figure 5C), as the interlayer is moved through the sample from the surface to greater depths, its signal is initially increasing, then peaking, and monotonously decreasing thereafter. Both the MC calculations and experimental results are in very good agreement in predicting and confirming this behavior. This effect is also in line with (but not necessitated by) the MC simulation results in Figures 1 and 2, evidencing that the range of probed depths captured through the 10%, 50% (median), and 90% quantiles ("probed channel") is gradually moving into greater depths with increasing spatial offset. In a similar fashion, the depth where the maximum signal is obtained is also gradually moving deeper with increasing spatial offset. At the photon level, this reflects the fact that photon pathways gradually statistically extend to greater depths with increasing spatial offset. This is because any propagation pathway close to the sample-to-air interface, despite constituting potentially a shorter distance to traverse, is subject to a high likelihood of crossing this boundary and causing photon loss. Therefore, such "shallow" photon trajectories are not the most "favored" by photons.

Absorption can however play a much more significant role[27,33] and thus can severely shorten the probed depths for all spatial offsets. This is illustrated in Figure S4, Supporting Information, for the polystyrene matrix (PS) with absorption coefficient μ_a = 0.0068 mm^{-1} (optical density OD = 0.0030

https://doi.org/10.1021/acs.analchem.1c00490
Anal. Chem. XXXX, XXX, XXX−XXX

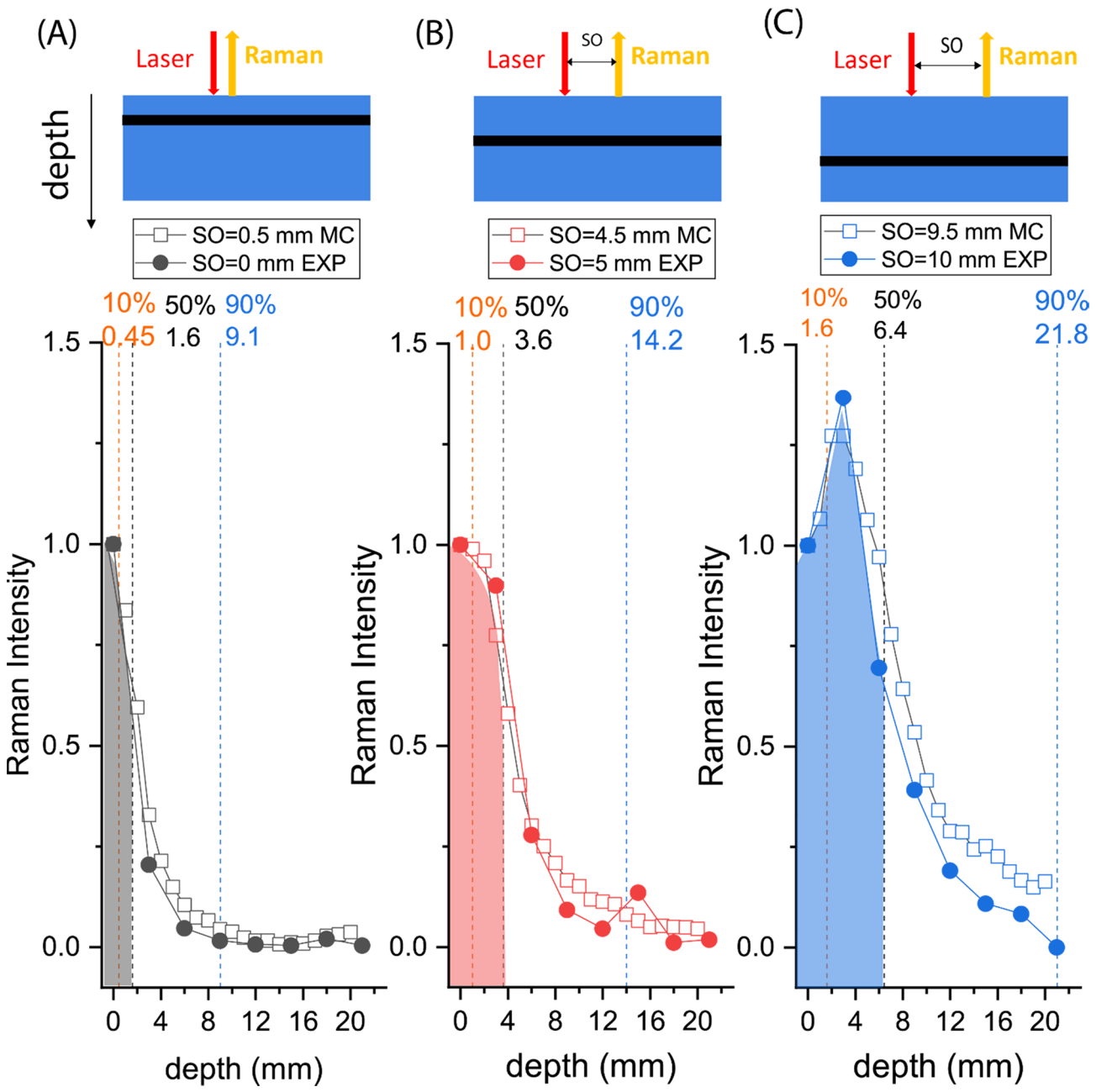

Figure 5. Normalized experimental Raman intensity decays of the 734 cm^{-1} PTFE Raman band (filled circles) of an interlayer buried in a PE turbid matrix, as a function of the interlayer depth, measured for different spatial offsets: (A) SO = 0 mm; (B) SO = 5 mm; (C) SO = 10 mm. The corresponding nearest numerical simulations are overlaid with the experimental data for each representative spatial offset (empty squares). On the MC results, a moving average of $n = 2$ point was applied. The vertical dash lines indicate calculated depths for 10% (orange), 50% (i.e., median, black), and 90% (blue) quantiles in mm for a non-absorbing turbid matrix with a transport length l_t = 1.6 mm for the selected spatial offsets.

mm^{-1}). Given that the median photon propagation distance for a spatial offset of 10 mm in a non-absorbing medium with a l_t = 0.6 mm (comparable to that of PS polystyrene value l_t = 0.588 mm) is ~580 mm, then in the presence of the polystyrene level of absorption, the overall light would be attenuated by a factor of 55 from the point of injection into the sample to its emergence at the detection site. In contrast, given that the PE nominal absorption coefficient of the matrix derived from the time-resolved NIR measurements is $\mu_a = 10^{-5}$ mm^{-1} and the median laser-Raman photon propagation distance is ~280 mm (Figure S5, Supporting Information) in a non-absorbing matrix of similar transport length l_t = 1.6 mm, then for a spatial offset of 9.5 mm, this amounts to the overall attenuation of light over its overall pathway by a factor of 1.0006, i.e., negligibly absorbed (although as stated above, it is noted that the value of the absorption coefficient for PE could be somewhat underestimated). The PS matrix therefore is expected to reduce the long photon propagation distance signals more than the shorter ones with the overall effect of a reduction in probed depths. The influence of absorption on probed depth is illustrated experimentally by moving the PTFE interlayer through a PS stack. Repeated MC simulations with absorption included reproduced the results reasonably well (see Figure S4, Supporting Information), although some underestimation of the degree of the reduction of the probed depth is present. Again, this is potentially due to the boundary

https://doi.org/10.1021/acs.analchem.1c00490
Anal. Chem. XXXX, XXX, XXX−XXX

effects, non-point-like geometry, and/or underestimated absorption coefficient used in the MC simulations. The Supporting Information provides several simple tests one can use to determine whether a probed medium exhibits a strong enough absorption to considerably reduce the probed depths, e.g., by comparing the observed Raman intensity decay rate with a spatial offset against the theoretical one derived under the assumption of no absorption present (see Figure S2, Supporting Information).

CONCLUSIONS

We presented a systematic study of the probed depth in SORS measurements for any particular spatial offset using Monte Carlo simulations. The analysis was performed under the assumption of no significant absorption being present and showed that the key parameter defining the scale of the problem is the reduced scattering coefficient μ_s' or the transport length l_t ($\mu_s' = 1/l_t$). Once the reduced scattering coefficient (or transport length) is accounted for, a probed depth can be determined for any specific SORS spatial offset using the results of these MC calculations. The predictions were tested using experimental data acquired from a PE matrix with negligible absorption, yielding satisfactory results. The study provides an important methodology for estimating probed depths in SORS studies, impacting a wide range of applications including biomedical, pharmaceutical, security, forensics, and cultural heritage.

ASSOCIATED CONTENT

Supporting Information

The Supporting Information is available free of charge at https://pubs.acs.org/doi/10.1021/acs.analchem.1c00490.

Raman spectra and optical properties of the model samples, role of absorption, and photon propagation distances (PDF)

AUTHOR INFORMATION

Corresponding Authors

Nick Stone − *School of Physics and Astronomy, University of Exeter, Exeter EX4 4QL, United Kingdom;* orcid.org/0000-0001-5603-3731; Email: N.Stone@exeter.ac.uk

Pavel Matousek − *Central Laser Facility, Research Complex at Harwell, STFC Rutherford Appleton Laboratory, UK Research and Innovation, Didcot OX11 0QX, United Kingdom;* orcid.org/0000-0003-0912-5339; Email: Pavel.Matousek@stfc.ac.uk

Authors

Sara Mosca − *Central Laser Facility, Research Complex at Harwell, STFC Rutherford Appleton Laboratory, UK Research and Innovation, Didcot OX11 0QX, United Kingdom;* orcid.org/0000-0001-9479-5614

Priyanka Dey − *School of Physics and Astronomy, University of Exeter, Exeter EX4 4QL, United Kingdom;* orcid.org/0000-0003-2896-7611

Marzieh Salimi − *School of Physics and Astronomy, University of Exeter, Exeter EX4 4QL, United Kingdom*

Benjamin Gardner − *School of Physics and Astronomy, University of Exeter, Exeter EX4 4QL, United Kingdom;* orcid.org/0000-0002-7223-9585

Francesca Palombo − *School of Physics and Astronomy, University of Exeter, Exeter EX4 4QL, United Kingdom;* orcid.org/0000-0001-6355-2601

Complete contact information is available at: https://pubs.acs.org/10.1021/acs.analchem.1c00490

Notes

The authors declare no competing financial interest.

ACKNOWLEDGMENTS

This work was supported by the Engineering and Physical Sciences Research Council grant EP/R020965/1.

REFERENCES

(1) Matousek, P.; Clark, I. P.; Draper, E. R. C.; Morris, M. D.; Goodship, A. E.; Everall, N.; Towrie, M.; Finney, W. F.; Parker, A. W. *Appl. Spectrosc.* **2005**, *59*, 393−400.

(2) Mosca, S.; Conti, C.; Stone, N.; Matousek, P. *Nat. Rev. Methods Primers* **2021**, *1*, 21.

(3) Matousek, P.; Morris, M. D.; Everall, N.; Clark, I. P.; Towrie, M.; Draper, E.; Goodship, A.; Parker, A. W. *Appl. Spectrosc.* **2005**, *59*, 1485−1492.

(4) Nicolson, F.; Kircher, M. F.; Stone, N.; Matousek, P. *Chem. Soc. Rev.* **2021**, *50*, 556−568.

(5) Martelli, F.; Binzoni, T.; Pifferi, A.; Spinelli, L.; Farina, A.; Torricelli, A. *Sci. Rep.* **2016**, *6*, 27057.

(6) Martelli, F.; del Bianco, S.; Ismaelli, A.; Zaccanti, G. *Spie B.* **2009**, 1365.

(7) Keller, M. D.; Wilson, R. H.; Mycek, M.-A.; Mahadevan-Jansen, A. *Appl. Spectrosc.* **2010**, *64*, 607−614.

(8) Matousek, P.; Conti, C.; Colombo, C.; Realini, M. *Appl. Spectrosc.* **2015**, *69*, 1091−1095.

(9) Martelli, F.; Binzoni, T.; Sekar, S. K. V.; Farina, A.; Cavalieri, S.; Pifferi, A. *Opt. Express* **2016**, *24*, 20382.

(10) Reble, C.; Gersonde, I.; Lieber, C. A.; Helfmann, J. *Biomed. Opt. Express* **2011**, *2*, 520.

(11) Akbarzadeh, A.; Edjlali, E.; Sheehy, G.; Selb, J.; Agarwal, R.; Weber, J.; Leblond, F. *J. Biomed. Opt.* **2020**, *25*, 105002.

(12) Martelli, F.; Contini, D.; Taddeucci, A.; Zaccanti, G. *Appl. Opt.* **1997**, *36*, 4600.

(13) Del Bianco, S.; Martelli, F.; Zaccanti, G. *Phys. Med. Biol.* **2002**, *47*, 4131−4144.

(14) Mosca, S.; Dey, P.; Salimi, M.; Gardner, B.; Palombo, F.; Stone, N.; Matousek, P. *Anal. Chem.* **2021**, *93*, 3386−3392.

(15) Liu, H.; Boas, D. A.; Zhang, Y.; Yodh, A. G.; Chance, B. *Phys. Med. Biol.* **1995**, 1983.

(16) Taroni, P.; Pifferi, A.; Torricelli, A.; Comelli, D.; Cubeddu, R. *Photochem. Photobiol. Sci.* **2003**, *2*, 124.

(17) Torricelli, A.; Pifferi, A.; Taroni, P.; Giambattistelli, E.; Cubeddu, R. *Phys. Med. Biol.* **2001**, *46*, 2227−2237.

(18) Jacques, S. L. *Phys. Med. Biol.* **2013**, *58*, R37−R61.

(19) Cheong, W. F.; Prahl, S. A.; Welch, A. J. *IEEE J. Quantum Electron.* **1990**, *26*, 2166−2185.

(20) Mosca, S.; Dey, P.; Salimi, M.; Palombo, F.; Stone, N.; Matousek, P. *Analyst* **2020**, *145*, 7623−7629.

(21) Mosca, S.; Dey, P.; Tabish, T. A.; Palombo, F.; Stone, N.; Matousek, P. *J. Biophotonics* **2020**, *13*, e201960092.

(22) Mosca, S.; Dey, P.; Tabish, T. A.; Palombo, F.; Stone, N.; Matousek, P. *Anal. Chem.* **2019**, *91*, 8994−9000.

(23) Jacques, S. L.; Wang, L. Monte Carlo Modeling of Light Transport in Tissue. In *Optical-Thermal Response of Laser-Irradiated Tissue. Lasers, Photonics, and Electro-Optics*; Springer, Boston, MA, 1995; pp 73−100, DOI: 10.1007/978-1-4757-6092-7_4.

(24) Das, B. B.; Liu, F.; Alfano, R. R. *Rep. Prog. Phys.* **1997**, *60*, 227.

(25) Brenan, C. J. H.; Hunter, I. W. *J. Raman Spectrosc.* **1996**, *27*, 561−570.

(26) Mosca, S.; Lanka, P.; Stone, N.; Konugolu Venkata Sekar, S.; Matousek, P.; Valentini, G.; Pifferi, A. *Biomed. Opt. Express* **2020**, *11*, 1697.
(27) Sekar, S. K. V.; Mosca, S.; Farina, A.; Martelli, F.; Taroni, P.; Valentini, G.; Cubeddu, R.; Pifferi, A. *Opt. Express* **2017**, *25*, 4585.
(28) Bashkatov, A. N.; Genina, E. A.; Tuchin, V. V. *J. Innov. Opt. Health Sci.* **2011**, *04*, 9−38.
(29) Mills, H. N. *J. Non-Cryst. Solids* **1982**, *47*, 27−46.
(30) Patterson, M. S.; Chance, B.; Wilson, B. C. *Appl. Opt.* **1989**, *28*, 2331−2336.
(31) Hall, C. Electrical and Optical Properties. In *Polymer Materials: An Introduction for Technologists and Scientists*; Macmillan Education UK: London, 1981; pp. 92−112. DOI: 10.1007/978-1-349-10187-0_4.
(32) Konugolu Venkata Sekar, S.; Dalla Mora, A.; Bargigia, I.; Martinenghi, E.; Lindner, C.; Farzam, P.; Pagliazzi, M.; Durduran, T.; Taroni, P.; Pifferi, A.; Farina, A. *IEEE J. Sel. Top. Quantum Electron.* **2016**, *22*, 406.
(33) Gardner, B.; Matousek, P.; Stone, N. *Analyst* **2021**, 1260.

https://doi.org/10.1021/acs.analchem.1c00490
Anal. Chem. XXXX, XXX, XXX−XXX